RSC Advances

ROYAL SOCIETY OF CHEMISTRY

www.rsc.org/advances

Adsorption characteristics and mechanism of sewage sludge-derived adsorbent for removing sulfonated methyl phenol resin in wastewater

Yucheng Liu,*,† Ju Chen,† Mingyan Chen,† Bo Zhang,† Danni Wu,† and Qixuan Cheng†

†School of Chemistry and Chemical Engineering, Southwest Petroleum University, Chengdu 610500, China

ABSTRACT

Sulfonated methyl phenol resin (SMP) is one of most popular organic additives in drilling fluid. It is difficult to treat drilling wastewater that contains SMP. Sewage sludge-derived adsorbent (SSA) was prepared by pyrolysis and activation of sewage sludge. Compared to other biochar and bentonitic adsorbents, the SSA possessed the highest adsorption capacity for SMP, with a removal capacity of 39.41 mg g^{-1}. The adsorption of SMP onto SSA was investigated by pH, ionic strength, SMP initial concentration, contact time and temperature. The Langmuir and Freundlich isotherm models were used to describe the adsorption equilibrium. The Langmuir monolayer adsorption capacity of SSA was estimated as 42.97 mg g^{-1}. The pseudo-first-order kinetic, pseudo-second-order kinetic and intra-particle diffusion kinetic model were employed to analyze the adsorption process of SMP onto SSA. The adsorption activation energy (E_a) was 23.95 kJ mol^{-1} at 25 - 40 °C, which implied the physisorption was more significant in the SMP-SSA system. The adsorption thermodynamics was evaluated, and the parameters such as the enthalpy (ΔH^0) was 14.41 kJ mol^{-1} and entropy (ΔS^0) was 58.64 J mol^{-1} K^{-1} at 100 mg L^{-1} SMP. The results indicated the SMP adsorption onto SSA was spontaneous and endothermic in nature. The excellent adsorption capacity for SMP indicates that the SSA could be a new promising low cost adsorbent for removal of SMP pollutants in drilling wastewater.

KEY WORDS

Sewage sludge; Adsorption; Sludge adsorbent; Sulfonated methyl phenol resin

1. Introduction

Sewage sludge can be used as a potential precursor for the production of adsorbent materials due to its carbon properties.[1,2] In recent years, considerable attention has been given to adsorbents derived from sewage sludge for the removal of pollutants. Some benefits include low potential cost and environmental sustainability. [3] The properties of the adsorbent and its affinity to different pollutants

are different due to the heterogeneous nature of raw sludges and the diversification of preparation processes.[1,2] Much research has been conducted on aqueous adsorption,[4] such as the uptake metals ions (Cu^{2+}, Ca^{2+}, Mg^{2+}, Cd^{2+}, Cr^{6+}, Hg^{2+}),[5-10] the removal of dye (methylene blue, acid yellow, alkaline black, acid red, naphthalene dye),[11-16] the uptake of pharmaceutical products (tetracycline, antibiotics, anticonvulsants),[17,18] and the adsorption of phenol and benzene derivatives (phenol, 4-chlorophenol, benzoic acid, 4-hydroxylbenzoic acid).[19-21] In addition, some authors have studied the adsorption of organic materials (phosphates, chemical oxygen demand (COD)) in wastewater onto sludge-derived adsorbents.[22,23] However, there have been few studies on the adsorption of large molecule organic pollutants on sewage sludge-derived adsorbent.

Sulfonated methyl phenol resin (SMP) is one of most popular organic additives in drilling fluid used in wells deeper than 3000 m. Some beneficial properties include, due to the good fluid loss, dispersion characters, and resistance to high temperature (up to 200 °C).[24-26] SMP is a type of polyelectrolytes that contains sulfonated methyl ($-CH_2SO_3^-$) in the molecular chain. The functional group enhances the hydrostability and solubility of SMP, and stabilizes the drilling fluid as a high content of suspended solid slurry.[27,28] Because these functional groups are hydrophilic and non-biodegradable, it is hard to remove SMP from wastewater by means of coagulation and microbiological methods, both of which are commonly used methods for wastewater treatment. According to Lv *et al*.,[29,30] the adsorption method was able to achieve a satisfactory result, but the adsorbent itself was expensive for wastewater treatment. So finding a low cost adsorbent for treatment of drilling wastewater is significant. Unfortunately, few studies have reported concerning SMP adsorption on sewage sludge-derived adsorbent, considering its potential low cost and hierarchical porosity.

It is meaningful and valuable to research the removal of SMP by sewage sludge-derived adsorbent in aqueous solution. The sewage sludge-derived adsorbent (SSA) was prepared by pyrolysis and activation of sewage sludge. SSA was then used to adsorb SMP in aqueous solution. This work focuses on the adsorption characteristics and mechanism of SMP onto SSA. We analyzed the influence of pH value and ionic strength on adsorption. Thermodynamic parameters were calculated to analyze the nature of adsorption. The kinetic and isotherm models for adsorption were investigated to understand the adsorption mechanism of SMP onto SSA.

2. Materials and experiment methods

2.1 Experiment Materials

Dewatered sewage sludge used in this study was collected from Jinhai Municipal Wastewater Treatment Plant in Chengdu, China, where wastewater treatment undergoes an activated sludge process. Sulfonated methyl phenol resin (SMP, CAS No.: 68201-32-1, Dry basis content: 88%), was purchased from Bazhou Sanyuan Petroleum Additives Corp., Xinjiang, China (industrial grade). $ZnCl_2$, $K_2Cr_2O_7$, $(NH_4)_2Fe(SO_4)_2{\cdot}6H_2O$, H_2SO_4, HCl and NaOH were purchased from Changzheng Chemical Corp., Chengdu, China (analytical grade). All of the required solutions were prepared with deionized water.

2.2 preparation of SSA

The collected sample was dried at 105 °C for 24 h， ground and sieved through a size of 50 - 70 mesh. It was then impregnated into 2.5 M $ZnCl_2$ solution at a ratio of 1:2.5 (dry sewage sludge (SS) : $ZnCl_2$ solution, wt : wt) and was stored for 24 h at room temperature. Subsequently, the supernatant liquid was removed and the impregnated SS was dried at 85 °C for 12 h. The sample was pyrolyzed in a box-type electronic heating furnace under a nitrogen atmosphere; it was heated at a ramp rate of 10 °C min^{-1} to reach 500 °C and then maintained for 60 min. After cooling down to room temperature, the pyrolyzed product was ground, sieved into less than 100 mesh, washed three times with 3 M hydrochloric acid solution, and then rinsed with deionized water until the pH was approximately 6 - 7. Finally, the product was dried at 105 °C for 12 h. The wheat straw and the walnut shell were pyrolyzed at 600 °C for 2 h, then washed, ground and dried by the same way of SSA. The biochars obtained were labeled as WRB (wheat straw biochar) and WEB (walnut shell biochar).

2.3 Characterization of SMP

Prior to the use, the SMP sample was further purified by deionized water, filtered through a 0.45 μm membrane, concentrated by reduced pressure distillation, and desiccated in an oven. The pH of SMP solution was varied using 0.1 M HCl and 0.1 M NaOH solutions. The surface charge of SMP molecular was characterized by the zeta potential in Zeta PALS 190 Plus (Brookhaven Instruments Corp., USA). Total Organic Carbon (TOC) and Chemical Oxygen Demand (COD) analyses were employed for quantitative detection of SMP in water. The TOC analysis was carried out by the TOC-VCPH analyzer (SHIMADZU corp., Japan), and the COD analysis was performed according to the dichromate-based COD protocol described in prior work.[31]

2.4 Characterization of SSA

The proximate analysis included moisture and ash contents were determined by ASTM D2867-09 (2014) and D2866-11 (2004).[32,33] Ultimate analysis was carried out in an Elementary Analyzer vario EL-Ⅲ(Elementar Corp., Germany) to determine C, H, N and S contents of the SS and SSA, and O content was calculated by difference. The SSA porous structure was determined by N_2 adsorption-desorption isotherms at -196 °C, which was obtained in a QUADRASORB SI automatic surface area and pore structure analyzer (Quanta Chrome Instrument Corp., USA). The functional groups of SS and SSA were determined using the WQF-520 FIRT spectra (Beijing Ruili Analytical Instrument corp., China). The energy dispersive X-ray spectroscopy (EDS) analysis of SSA surface was carried out by a ZEISS EVO MA 15 scanning electron microscope (Carl Zeiss corp., Germany). The Boehm titration was employed to quantitatively determine organic oxygen-containing functional groups on SSA surface.[34] 0.2 g of SSA was placed into 25 mL of the 0.05 M base solution ($NaHCO_3$, Na_2CO_3, or NaOH). After shaking for 24 h to reach equilibrium, the SSA was filtered to separate from solution. Then, the excess base was determined by back titration with 0.05 M HCl solution. The pH of point of zero charge (pH_{pzc}) of SSA was determined by pH drift method.[35] 0.1 g of SSA was added into a 20 mL of solution with an initial pH ranged from 1 to 11. After shaking for 24 h, the final pH was determined. When the final pH was equal to the pH initial, the value was the pH_{pzc} of SSA.

2.5 Adsorption experiments

Adsorption experiments were performed as follows: 50 mL SMP solution and 0.25 g SSA were added into a 150 mL Erlenmeyer flask with a ground stopper. The flask was placed in a water bath and mechanical shaker at a speed of 240 rpm. After shaking for 50 h, the flask was taken out and the sample was filtered to separate the adsorbent from solution. For each experiment, the blank tests was carried out with deionized water, and the initial concentration of SMP solution (C_0) was determined after the shaker test without adsorbent. The residual SMP concentration (C_e) in solution was obtained after deducting blank value.

The SMP adsorption capacity (q_e, mg g^{-1}) was calculated as follows:

$$q_e = \frac{(C_0 - C_e)}{m} \quad (1)$$

where, C_0 is the initial concentration of SMP solution (mg L^{-1}), C_e is the residual SMP concentration at equilibrium (mg L^{-1}), and m is the SSA dosage (g L^{-1}).

To study the effect of pH on SMP adsorption onto SSA, the experiments were performed at different pH levels (varying from 1.2 to 8.3), with an initial SMP

concentration of 300 mg L^{-1} and an adsorbent dosage of 4 g L^{-1}. The influence of ionic strength was investigated by increasing NaCl concentration from 0.01 to 0.1 g L^{-1}. At different temperatures (10 °C, 25 °C and 40 °C), the adsorption experiments were performed at predetermined time intervals. For adsorption isotherms, the experiments were performed at various temperatures (10 °C, 20 °C, 30 °C and 40 °C), with different initial concentrations of SMP solution (50 - 500 mg L^{-1}). For each experiment, the test was repeated three times, and the average value was reported. The determined experiment results agreed to within 5% of the relative standard deviation.

3. Results and discussion

3.1 SMP characterization

The SMP used was a mixture of resin synthetic products with different degrees of polymerization, and the main molecular structure is presented in Fig. 1. The SMP molecular chain is formed by phenolic rings, which is linked with methylene via *ortho*-positions. The *para*-positions are substituted by hydroxyl-methyls, and the sulfonated methyls are linked on the benzene ring, which mainly occur on the head of the molecular chain.[26,36] Since SMP was synthesized in the basic environment, the sulfonated methyl and phenolic hydroxyl were ionized with a pH of 8.64 at a concentration of 300 mg L^{-1}. The SMP had the rigid aromatic ring, and formed molecule aggregates by hydrophobic effect in water. Furthermore, the aggregates surface formed a hydration layer by the hydrogen bonding formed between hydrophilic groups (sulfonated methyl, phenolic hydroxyl) and water molecules, and caused a large hydrodynamic diameter (about 100 nm).[36] From DLVO theory, the stability of colloid system depends on the repulsion and attraction force between colloid particles. Zeta potential was related to the electrostatic interaction, the high absolute value of zeta potential (-39 mv, at SMP concentration of 300 mg L^{-1}) led to a higher repulsion between SMP aggregates, the SMP solution was stable.

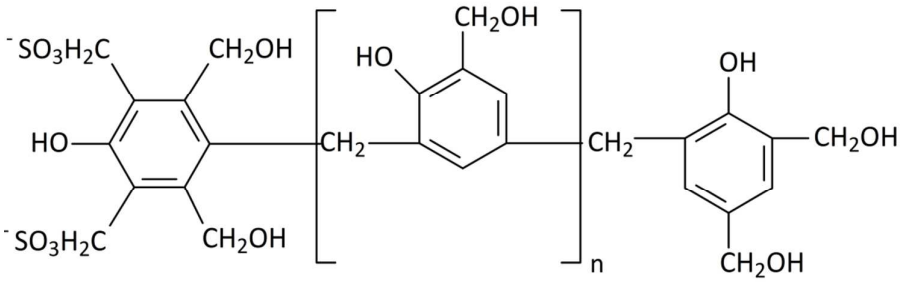

Fig. 1 Structure formula of SMP, n is an integer ranged from 0 to 7.

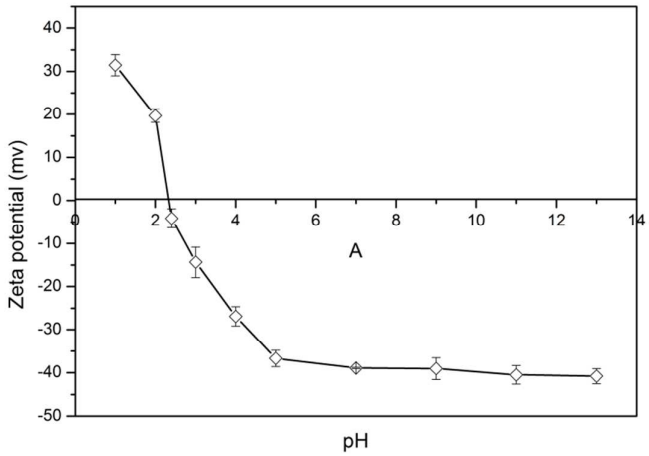

Fig. 2 The Zeta potential of SMP as a function of solution pH, SMP concentration: 300 mg L^{-1}.

166 The solution pH affected the protonation and ionization of the groups, hence, it
167 could change the zeta potential of the SMP molecule aggregates. As showed in Fig. 2,
168 when the pH decreased from 7 to 1, the zeta potential of the SMP aggregates
169 transformed from negative to positive. Increasing hydrogen ion diffused into the
170 stern layer of SMP colloid particles, and adsorbed selectively onto the ionized groups
171 of SMP. As a result, the zeta potential of SMP aggregates became reverse. Specially,
172 when pH reduced approximately to 2.3, zeta potential reached 0, the isoelectric
173 point of the SMP molecule aggregates was observed. At the isoelectric point, the
174 electrostatic interaction was minimum, the SMP aggregates was liable to coagulation
175 due to collision.

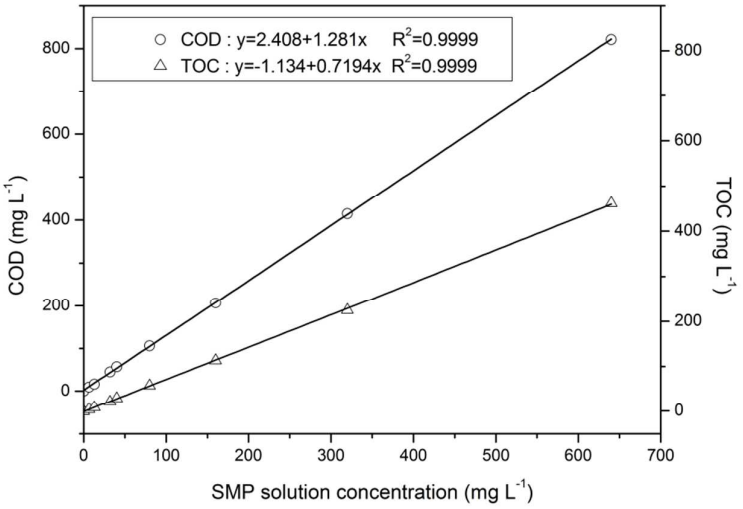

Fig. 3 Calibration curve of aqueous SMP by COD and TOC analysis.

176 The feasibility of utilizing Total Organic Carbon (TOC) and Chemical Oxygen
177 Demand (COD) analyses for the quantitative detection of SMP in aqueous samples

was investigated. SMP solutions containing 6.4 - 640 mg L^{-1} were tested with TOC and COD, and the results are presented in Fig. 3. Both the Coefficient of determinations (R^2) of the two standard curves is 0.9999, which indicates that the TOC and COD measurements for SMP quantification were suitable and feasible.

3.2 SSA characterization

The proximate and ultimate analysis results of SS and SSA are presented in Table 1. The SS contained the carbon content of 33.82%, which implied that the sludge could serve as a precursor to carbon. According to ultimate analysis, the SSA contained more C, N and S contents, but had a decrease in the H and O contents. That was a result of the dehydration of the activating agent that influenced the pyrolytic decomposition, and lower ash content was owing to the acid washing.[37] The N, H, S and O contents were varied, which might be a result of the various functional groups.

Table 1

Characterization of proximate and ultimate analysis for sewage sludge (SS) and sewage sludge-derived adsorbent (SSA)

Sample	Proximate Analysis (%)		Ultimate Analysis (%)				
	Moisture	Ash	C	H	N	S	O[a]
SS	2.84	32.53	33.82	4.73	6.00	1.93	20.99
SSA	2.42	27.92	43.15	4.12	6.25	2.87	15.69

[a] By difference, O = 100 – C – H – N – S – Ash.

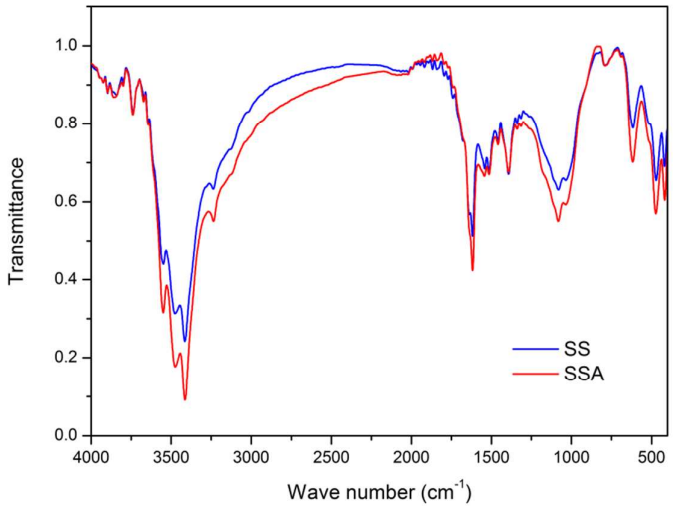

Fig. 4 FTIR spectroscopy of SS and SSA.

The absorption bands and peaks on the FTIR spectrum were often used to indicate the existence of functional groups on the adsorbent surface.[38] Fig. 4 shows

the FTIR spectrums of the SSA and SS with the similar peaks but different strength, indicating the presence of similar functional groups on the surface.[39] The broad band between 1000 and 1050 cm^{-1} for the SS and SSA exhibited C–O stretching absorption[3] and the shoulder at 1050-1090 cm^{-1} was assigned to the structure of either Si–O–Si or Si–O–C groups.[40] It is clear that a stronger and broader band (at 3300-3550-cm^{-1}) could be ascribed to the O–H stretching of alcohols or the N–H stretching absorption of the amines.[41] The weak band appearing at the 615 - 790 cm^{-1} and 1515 - 1550 cm^{-1} regions, also confirmed the presence of $-NH_2$.[42] The bands appear at 3800 and 3754 cm^{-1}, indicating free OH groups in the carboxyl group.[43] Another band was observed at 1390 and 1450 cm^{-1} and was assigned to O–H bending vibration in carbonates or carboxyl-carbonates.[44] The peak at 1616 cm^{-1} was observed in Fig. 4, which can be attributed to the C=O stretching absorption by the carboxyl anion, and the C=C stretching conjugating with another C=C bond, a C=O bond, or an aromatic nucleus.[41] In fact, the C=C stretching absorption (at approximately 1600 cm^{-1}) was frequently observed in the study of carbonaceous materials.[45,46] In conclusion, the main functional groups on the surface of the SSA are –C=O, OH, $-NH_2$, C=C and Si–O–Si or Si–O–C.

Table 2

Porous structure of the sewage sludge-derived adsorbent (SSA)

S_{BET}[a]($m^2\ g^{-1}$)	215.6	V_{Total}[d]($cm^3\ g^{-1}$)	1.960
D_{meso}[b](nm)	3.72	V_{Meso}[e]($cm^3\ g^{-1}$)	0.058
D_{micro}[c](nm)	0.37	V_{Micro}[f]($cm^3\ g^{-1}$)	0.013

[a] BET surface area, by BET method.

[b] Average mesopore diameter, by BJH method.

[c] Average micropore diameter, by HK method.

[d] Total pore volume at $P/P_0 = 0.98$.

[e] Volume of mesopores, by BJH method.

[f] Volume of micropores, by DR method.

Table 3

Contents of oxygen-containing functional groups from Boehm titration and pH of point of zero charge of SSA

Carboxyl (meq g^{-1})	0.720	Total acid (meq g^{-1})	1.285
Lactones (meq g^{-1})	0.303	Total base (meq g^{-1})	—[a]
Phenolic hydroxyl (meq g^{-1})	0.262	pH_{pzc}	3.48

[a] Not determined.

Table 2 showed that the SSA sample had a BET surface area of 215.6 m^2 g^{-1}, with a low volume of micropores (0.013 cm^3 g^{-1}), and a relatively high mesopores (0.058 cm^3 g^{-1}), which was owing to the fabricating-pore effect of $ZnCl_2$.[21] Similarly, some studies on SSA reported the degree of micropores was generally not high. Considering the adsorbate molecular size,[47,48] Yu and Zhong reported the relatively high mesopores of SSA facilitated the adsorption large organic matter.[49] With the pH_{pzc} of 3.48 (Fig .S1), the acidic surface properties of SSA was caused by the presence of acid oxygen-containing functional groups quantified by Boehm titration in Table 3. The high carboxyl group content was determined of 0.720 meq g^{-1}, and lactones and phenolic hydroxyl groups were 0.303 and 0.262 meq g^{-1}, respectively. The pore structure and surface functional groups might give a special adsorption capacity for the SSA in removing organic pollutants.

3.3 Effect of the solution pH and ionic strength

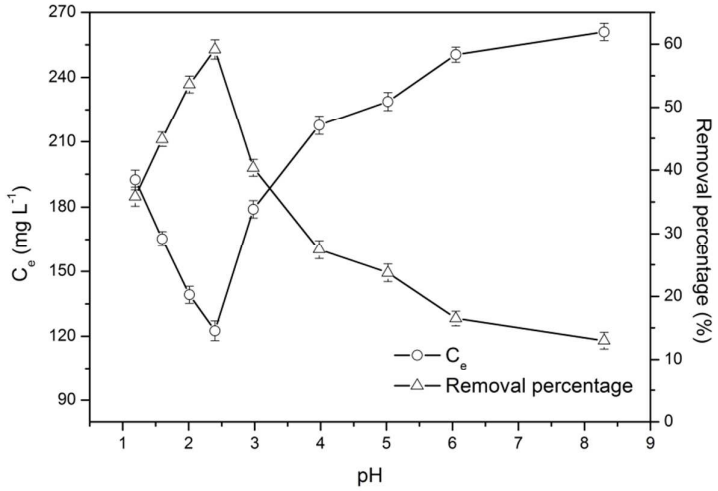

Fig. 5 Effect of the solution pH on SMP adsorption onto SSA at given conditions: C_0: 300 mg L^{-1}, SSA dosage: 4 g L^{-1}, contact time: 50 h.

The initial pH of the adsorption solution is a critical parameter.[50] The effect of pH on the SMP adsorption onto SSA was studied over the pH range of 1.2 - 8.3, and the result is shown in Fig. 5. The maximal removal percentage was observed at pH of 2.4. This can be explained by the effects of surface charge of the SSA and SMP. At pH of 2.4, the zeta potential of SMP aggregates was negative in Fig. 2, the SSA surface was protonated partly from Fig. S1. Thus, the electrostatic interaction between SSA and SMP was attraction. Moreover, the hydrogen bond was weakened due the decrease of hydrogen acceptors in acid solution. As a result, the hydration layer on SMP aggregates surface can be broken, which conduced to SMP molecules access to adsorption sites on SSA surface.[51] Overly acidic or basic environment led to a

decrease of SMP removal percentage, it might be due to increasing repulsion between SMP aggregates.

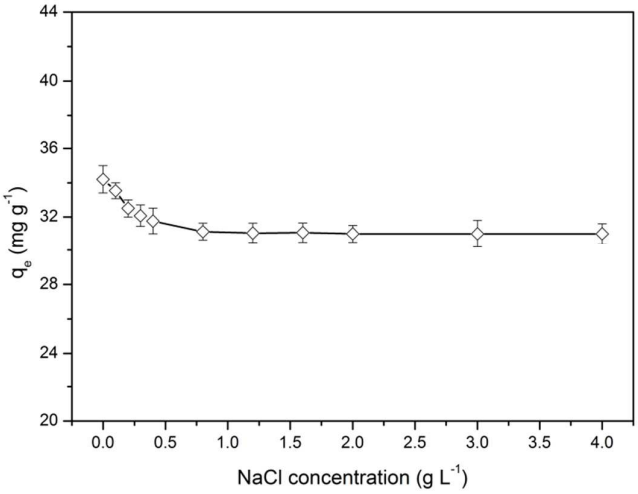

Fig. 6 Effect of the ionic strength on SMP adsorption onto SSA at given conditions: C_0: 300 mg L^{-1}, pH 2.4, SSA dosage: 5 g L^{-1}, contact time: 50 h.

The effect of the ionic strength on the removal of SMP was studied by increasing sodium chloride concentrations, and the results are presented in Fig. 6. As NaCl concentration in solution increased from 0 to 0.8 g L^{-1}, a decrease of 9.0 % in the removal rate of SMP was observed. Since then, as the NaCl increased, the removal rate no longer reduced, which indicated the ionic strength had a negative effect on the SMP adsorption onto SSA, within a small range. The increasing Na^+ can compress the electrical double layer of SMP aggregates, which influenced the surface charge of SMP aggregates. The electrostatic attraction between SMP and SSA was decreased due to the increasing ionic strength.[52,53] Moreover, the result could be attributed to the competition between SMP and background electrolyte. The adsorption behavior contained the specific and non-specific adsorption, and the ionic strength could influence the activity coefficients of adsorbates.[54] The Cl^{-1} can form competition adsorption with SMP on SSA surface adsorption sites, which reduced the SMP adsorption onto SSA.

3.4 Adsorption kinetics of SMP adsorption onto SSA

To analyze the process of the SMP adsorption onto SSA, the kinetic experimental data were fitted to three models: pseudo-first-order kinetic model, pseudo-second-order kinetic model and intra-particle diffusion kinetic model.[55,56]

Pseudo-first-order kinetic model

The equation of the Pseudo-first-order kinetic model expression is as follows:

$$\ln(q_1 - q_t) = \ln q_1 - k_1 t \quad (2)$$

where t is adsorption time (h), q_t is the adsorption quality of SMP on SSA at various time t (mg g^{-1}), q_1 is the adsorption quality of SMP on SSA at equilibrium (mg g^{-1}) for pseudo-first-order kinetic model, and k_1 is the pseudo-first-order rate constant (h^{-1}).

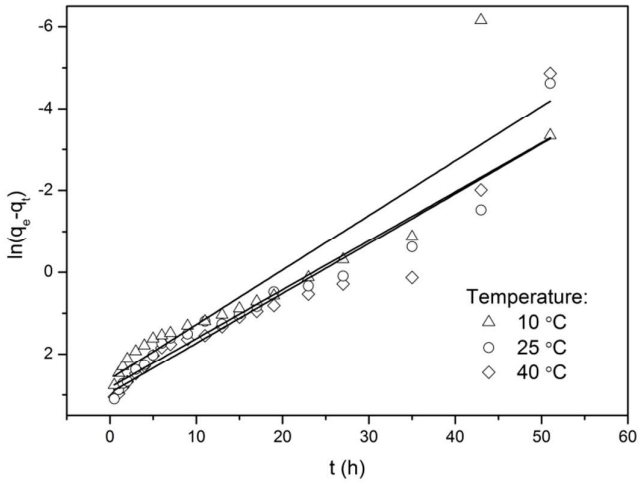

Fig. 7 Pseudo-first-order kinetic model for SMP adsorption onto SSA at 10 °C, 25 °C and 40 °C.

Fig. 7 shows the straight-line plots of $\ln(q_e - q_t)$ versus t for the pseudo-first-order model. The values of $q_{1,\mathrm{cal}}$ and k_1 were calculated by finding the intercept and slope. The estimated values of $q_{1,\mathrm{cal}}$ from the pseudo-first-order model and q_e values (from experiment) are summarized in Table 4.

From Table 4, there was a large gap of the equilibrium adsorption quantity between estimated ($q_{1,\mathrm{cal}}$) and experimented (q_e) values. Considering the low value of R^2 (0.8367 - 0.9320), it is suggested that the kinetics of SMP adsorption on SSA is less likely fitting the pseudo-first-order kinetic model.

Pseudo-second-order kinetic mode

The pseudo-second-order kinetic model is presented as:

$$\frac{t}{q_t} = \frac{1}{q_2^2 k_2} + \frac{t}{q_2} \quad (3)$$

where t is adsorption time (h), q_t is the adsorption quality of SMP on SSA at various time t (mg g^{-1}), q_2 is the adsorption quality of SMP on SSA at equilibrium for the pseudo-second-order kinetic model (mg g^{-1}), and k_2 is the pseudo-second-order rate constant (g mg^{-1} h^{-1}).

In the same way, $q_{2,\mathrm{cal}}$ and k_2 were calculated by the slope and intercept of the straight-line plots of t/q_t versus t for the pseudo-second-order model. These results are presented in Fig. 8 and Table 4.

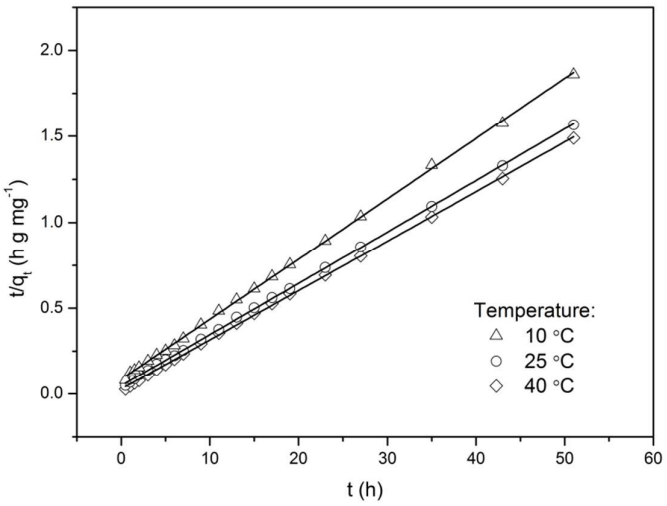

Fig. 8 Pseudo-second-order kinetic model for SMP adsorption onto SSA at 10 °C, 25 °C and 40 °C.

Table 4

Adsorption kinetic parameters at different temperatures for different models

T(°C)	q_e, (mg g^{-1})	Pseudo-first-order kinetic model			Pseudo-second-order kinetic mode		
		$q_{1,cal}$(mg g^{-1})	k_1(h^{-1})	R^2	$q_{2,cal}$(mg g^{-1})	k_2(g mg^{-1} h^{-1})	R^2
10	27.40	19.20	0.1219	0.9069	28.55	0.01430	0.9996
25	32.56	16.77	0.1196	0.9320	33.44	0.01884	0.9998
40	34.26	13.64	0.1334	0.8367	34.75	0.02993	0.9996

The correlation coefficient values (R^2) were applied to determine the goodness of fit between the kinetic models and the experimental data. From Fig. 7, Fig. 8, and Table 4, it is clear that the pseudo-second-order kinetic model fit the experimental data very well. The R^2 of the pseudo-second-order kinetic model (0.9996 - 0.9998) was higher than the first-order model (0.8367 - 0.9320) at different temperatures. Moreover, estimates equilibrium adsorption quantity ($q_{2,\mathrm{cal}}$) and experimental values (q_e) were similar at the corresponding temperature. Therefore, it may be concluded that the pseudo-second-order model is better than the first-order model to explain the adsorption behavior of SMP onto SSA. Hence, the SMP adsorption process is, not only related to the concentration of the SMP concentration, but also the SSA dosage.[56]

Intra-particle diffusion kinetic model

The intra-particle diffusion kinetic model is given as:

$$q_t = k_i t^{0.5} + I \quad (4)$$

where t is adsorption time (h), q_t is the adsorption quality of SMP on SSA at

various time t (mg g^{-1}), k_{i} is the intra-particle diffusion rate constant (mg g^{-1} h$^{-0.5}$), and I is the intercept for the intra-particle diffusion kinetic model (mg g^{-1}). I and k_i were calculated by the straight-line plots of q_t versus $t^{0.5}$ and are given in Table 5.

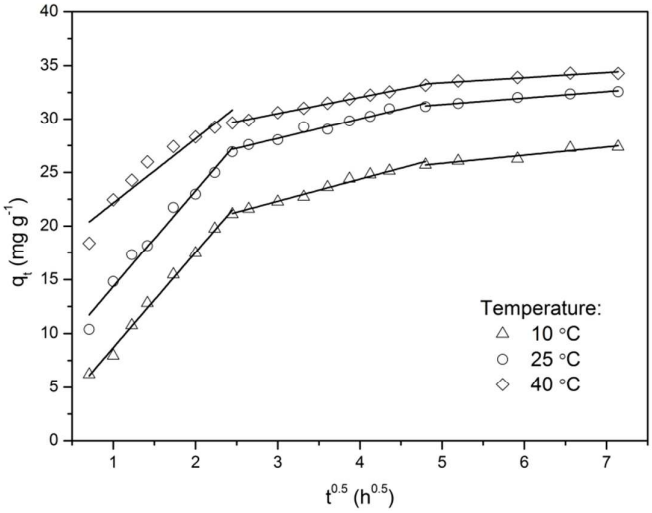

Fig. 9 Intra-particle diffusion kinetic model for SMP adsorption onto SSA at 10 °C, 25 °C and 40 °C.

Table 5

Intra-particle diffusion kinetic model parameters at different temperatures

T(°C)	The sharp increase stage			The gradual increase stage			The equilibrium stage		
	$k_{i,1}$ (mg g^{-1} h$^{-0.5}$)	I_1 (mg g^{-1})	R^2	$k_{i,2}$ (mg g^{-1} h$^{-0.5}$)	I_1 (mg g^{-1})	R^2	$k_{i,3}$ (mg g^{-1} h$^{-0.5}$)	I_1 (mg g^{-1})	R^2
10	8.829	-0.1445	0.9975	2.061	16.12	0.9839	0.7609	22.04	0.9141
25	8.919	5.427	0.9778	1.839	22.66	0.9633	0.6040	28.34	0.9706
40	6.007	16.13	0.9007	1.517	25.96	0.9968	0.4787	31.00	0.8932

Fig. 9 shows the intra-particle diffusion plots contained three segments: the sharp increase stage, the gradual increase stage and the equilibrium stage. In the sharp increase stage, the amount of adsorption of SMP onto SSA increased rapidly, within the first 6 h. This was owing to the instantaneous or the external surface adsorption.[19] The gradual increase stage (6.0 - 23 h) was attributed to intra-particle diffusion, and the adsorption increased gradually over time. The equilibrium stage was after 23 h, where adsorption reached equilibrium and intra-particle diffusion slowed down. The straight lines of the gradual increase and equilibrium stages no passed through the origin, which suggests that intra-particle and film diffusion were

306 occurring simultaneously in the adsorption process.[50]

307 *3.5 Adsorption isotherm model*

308 The equilibrium adsorption isotherm is one of the most important data to
309 interpret the mechanism of the adsorption systems.[57] In this study, the Langmuir and
310 Freundlich isotherm equations were used to describe the mechanism of SMP loading
311 on the SSA in solution at different temperatures.

312 The Langmuir isotherm model is based on the theory of molecular motion and
313 the derived monolayer adsorption assumption, which proposes that the adsorption
314 sites are distributed homogeneously on the surface of the adsorbent.[50] The Langmuir
315 isotherm model is one of the most frequently employed models because of its
316 simplicity and fits very well with experimental data. The equation is expressed as:

317 $$q_e = \frac{q_m C_e b}{1+bC_e} \quad (5)$$

318 where C_e is the residual SMP concentration at equilibrium (mg L^{-1}), q_e is the
319 adsorption quality of SMP on SSA at equilibrium (mg g^{-1}), q_m is the monolayer
320 adsorption capacity of SMP on SSA estimated by Langmuir model (mg g^{-1}), and b is
321 the Langmuir constant (L mg^{-1}).

322 The Freundlich isotherm equation is an empirical exponential equation and is
323 valid for adsorption of heterogeneous surfaces.[57] The model assumes that the
324 adsorption capacity is relevant to the adsorbate concentration at equilibrium.[50] The
325 equation of Freundlich isotherm model is represented as:

326 $$q_e = K_F C_e^{1/n} \quad (6)$$

327 where C_e is the residual SMP concentration at equilibrium (mg L^{-1}), q_e is the
328 adsorption quality of SMP on SSA at equilibrium (mg g^{-1}), K_F is the Freundlich
329 constant (mg g^{-1}(mg L^{-1})$^{-1/n}$), and n is the heterogeneity factor of the Freundlich
330 isotherm model. When $1/n$ value is in the range from 0.1 to 1, the adsorption
331 process is favorable.[58]

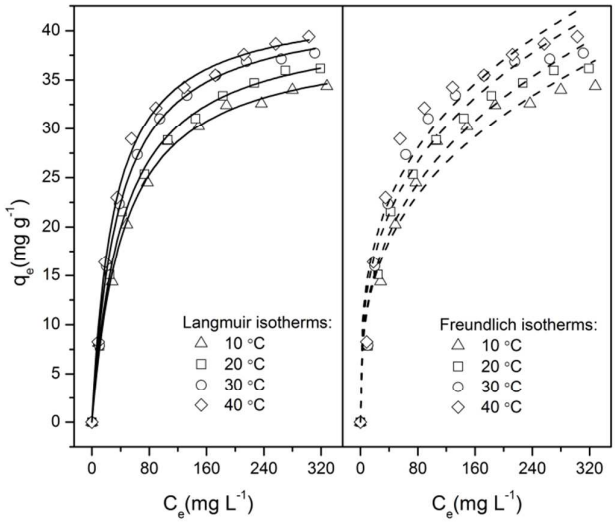

Fig. 10 Langmuir and Freundlich isotherms for SMP adsorption onto SSA, SSA dosage: 5 g L^{-1}, pH 2.4, contact tome 50 h, temperature: 10 ˚C, 20 ˚C, 30 ˚C, 40 ˚C.

Table 6

Langmuir and Freundlich isotherm constants for SMP adsorption onto SSA at 10 ˚C, 20 ˚C, 30 ˚C and 40 ˚C

T (◦C)	Langmuir isotherm			Freundlich isotherm		
	R^2	q_m(mg g^{-1})	b(L mg^{-1})	R^2	K_F(mg g^{-1} (L mg^{-1})$^{1/n}$)	n
10	0.9960	39.31	0.02257	0.9654	5.484	3.034
20	0.9980	41.03	0.02349	0.9672	5.558	2.963
30	0.9972	42.58	0.02786	0.9489	6.603	3.143
40	0.9969	42.97	0.03284	0.9513	7.379	3.283

Fig. 10 presents the Langmuir and Freundlich adsorption isotherms of SMP adsorption onto SSA at 10 ˚C, 20 ˚C, 30 ˚C and 40 ˚C, respectively, and the parameters were calculated and are summarized in Table 6. The correlation coefficients (R^2) of Langmuir isotherms (0.9960 - 0.9980) were higher than Freundlich isotherms (0.9513 - 0.9672). This suggests that Langmuir isotherm model has a higher fitting degree with experimental data. The Langmuir model explained experimental data better than the Freundlich model. It is concluded that the adsorption SMP onto SSA conformed to monolayer adsorption. In the Langmuir model, the constant (b) was defined as the ratio of the rate constant between adsorption and desorption rate constants and was related to the adsorption capacity. As the temperature increased from 10 ˚C to 40 ˚C, the value b respectively increased from 0.02257 to 0.03284 L mg^{-1}. Similar to b, the monolayer adsorption capacity (q_m) increased with increasing temperature. The q_m value reached a maximum (42.97 mg g^{-1}) at 40 ˚C, implying

that the adsorption sites for SMP increased with an increase of temperature. The results also suggest that the adsorption SMP onto SSA was favorable and endothermic.[58] The thermodynamic parameters will be discussed in detail in the following section.

3.6 Thermodynamic analyses

In this study, to investigate the impact of temperature on the thermodynamic characteristics of SMP adsorption onto SSA, kinetic experiments and isothermal experiments data were analyzed. The results from kinetic experiments are summarized in Table 4. The conclusion was that the pseudo-second-order model was reasonably applied in the SMP-SSA system. As the temperature increased, the adsorption rate constant (k) increased. The effects of temperature on k can be represented by the Arrhenius equation:[59]

$$k = Ae^{-\frac{E_a}{RT}} \quad (7)$$

where E_a is the adsorption activation energy in the SMP-SSA system (kJ mol^{-1}), R is the gas constant (8.31 J (mol K)$^{-1}$), T is the solution temperature (K), A is the pre-exponential factor, and k is the rate constant, in this case, pseudo-second-order rate constant. The adsorption activation energy of the SMP-SSA system was determined by the k values and the corresponding temperatures, using the equation as follows:

$$\ln\frac{k_1}{k_2} = \frac{E_a(T_1-T_2)}{RT_1T_2} \quad (8)$$

The adsorption activation energy (E_a) values were calculated. The E_a value was 23.95 kJ mol^{-1} at 25 - 40 °C, but 12.90 kJ mol^{-1} at 10 - 25 °C. Higher temperatures resulted in a larger E_a value, implied the SMP adsorption onto SSA was endothermic in nature. According to Nollet et al.,[59] the low E_a (5 - 40 kJ mol^{-1}) was characteristic of physisorption. Therefore, the SMP adsorption onto SSA was a result of physical adsorption.

Thermodynamic parameters of adsorption such as the Gibb's free energy (ΔG^0), enthalpy (ΔH^0) and entropy (ΔS^0) changes were calculated from the isothermal experiment data using the Eqs (9) and (10):[50]

$$\Delta G^0 = \Delta H^0 - T\Delta S^0 \quad (9)$$

$$\ln\frac{q_e\, m}{C_e} = \frac{\Delta S^0}{R} - \frac{\Delta H^0}{R\,T} \quad (10)$$

where m is the SSA dosage (g L^{-1}), C_e is the residual SMP concentration at equilibrium (mg L^{-1}), q_e is the adsorption quality of SMP on SSA at equilibrium (mg g^{-1}), R is the gas constant (8.31 J (mol K)$^{-1}$), and T is the solution temperature (K).

Eq (10) indicates that a graph of $\ln q_e\, m/C_e$ vs $1/T$ would yield a straight line, and the values of ΔH^0 and ΔS^0 can be estimated from the slope and intercept. The Enthalpy determination curves are presented in Fig. 11, and the values of ΔG^0, ΔH^0 and ΔS^0 are listed in Table 7.

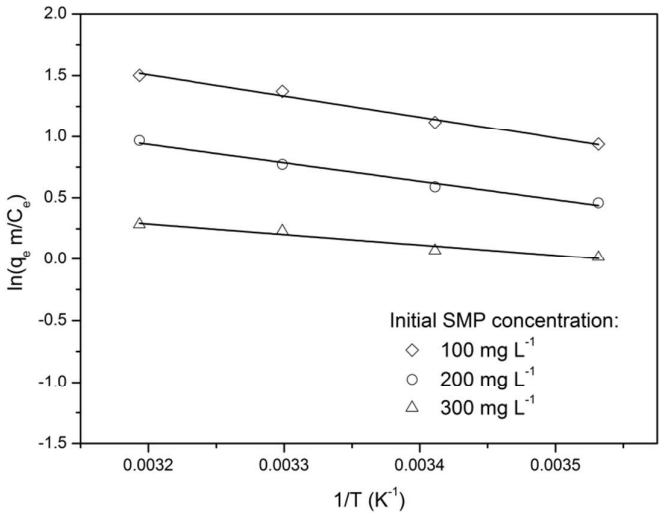

Fig. 11 Enthalpy determination curves for SMP adsorption onto SSA at different initial SMP concentrations.

Table 7

Thermodynamic parameters for SMP adsorption onto SSA at different initial SMP concentrations and temperatures

Initial concentration	ΔH^0	ΔS^0	ΔG^0(J mol^{-1} K^{-1})			
(mg L^{-1})	(kJ mol^{-1})	(J mol^{-1} K^{-1})	283 K	293 K	303 K	313 K
100	14.41	58.64	-2.19	-2.77	-3.36	-3.94
200	12.48	47.71	-1.02	-1.50	-1.98	-2.45
300	7.132	25.21	-0.0024	-0.25	-0.51	-0.76

According to Kara *et al.*,[60] the ΔH^0 value of physisorption was less than 40 kJ mol^{-1}. From Table 7, the ΔH^0 values were positive (7.132 - 14.41 kJ mol^{-1}) and were higher at a lower SMP initial concentration. This suggests the adsorption of SMP onto SSA was a physisorption process and was endothermic in nature. Moreover, the low ΔH^0 values implied a loose bonding between the SMP molecule aggregates and the SSA surface.[61] The value of ΔS^0 was positive (25.21 - 58.64 J mol^{-1} K^{-1}), suggesting that the degree freedom increased in the SMP-SSA system. The negative values of ΔG^0 support the fact that the adsorption of SMP onto SSA was spontaneous. Moreover, the negative ΔG^0 value was higher at lower SMP initial concentration

and higher temperature, indicating that the adsorption was more spontaneous. When the temperature increased from 10 ˚C to 40 ˚C, ΔG^0 became a higher negative value. At the same time, the monolayer adsorption capacity increased from 39.31 mg g^{-1} to 42.97 mg g^{-1}. The results further support that physisorption was more significant in the SMP-SSA system, which is in accordance with the conclusion from E_a.

3.7 Adsorption performance comparison

The adsorption capacities of SSA for removal of SMP have been compared with other adsorbents reported in literature, and the result was listed in Table 8. The SMP adsorption capacity was reported in the form of maximum adsorption capacities in experiments. At the same adsorption conditions, the adsorption amounts of WEB and WRB were 7.39 and 15.43 mg g^{-1}, far below SSA of 39.41 mg g^{-1}. It indicated that the SMP adsorption capacity was highly dependent on the raw materials of activated carbon, which might be related to the pore structure and surface functional groups of adsorbent. Yan studied the SMP adsorption onto the bentonitic clay, found the SMP adsorption capacity on bentonitic clay was highly depend on ionic strength. After added 15% NaCl, Yan found that the adsorption capacity increased from 8.0 to 28.9 mg g^{-1}. [62] Similarly, Eren *et al.* suggested that salt ions forced dye molecules to aggregate on the modified sepiolite surface.[63] The SMP adsorption capacity of the bentonitic clay was a relatively high value, which might be contributed to the special structure of mineral material. According to Grant and King, the presence of metals on the adsorbent surface can promote the surface polymerization that phenolic compounds produce polymeric compounds by oxidative coupling reactions on the carbon's surface.[64]

Table 8

Summary of adsorption of SMP by similar adsorbents

Adsorbents	Experimental condition	SMP adsorption (mg g^{-1})	Refs.
WEB	pH=2.4, T=40 ˚C, C(SMP)=500 mg L^{-1}, Adsorbent dosage=5.0 g L^{-1}, C(NaCl)=0 g L^{-1}	7.39	This work
WRB	pH=2.4, T=40 ˚C, C(SMP)=500 mg L^{-1}, Adsorbent dosage=5.0 g L^{-1}, C(NaCl)=0 g L^{-1}	15.43	This work
SSA	pH=2.4, T=40 ˚C, C(SMP)=500 mg L^{-1}, Adsorbent dosage=5.0 g L^{-1}, C(NaCl)=0 g L^{-1}	39.41	This work
Bentonitic clay	pH=8.0, T=25 ˚C, C(SMP)=16670 mg L^{-1}, Adsorbent dosage=40 g L^{-1}, C(NaCl)=0 g L^{-1}	8.0	62

Bentonitic clay	pH=8.0, T=25 °C, C(SMP)=16670 mg L^{-1}, Adsorbent dosage=40 g L^{-1}, C(NaCl)=150 g L^{-1}	28.9	62

Table 9

The EDS analysis of SSA surface inorganic substance

	Inorganic substance of SSA surface							
SSA surface element	Si	Al	Fe	Cl	K	Ca	Zn	Mg
Percentage in total(%)	8.57	2.96	2.02	1.33	1.03	0.53	0.48	0.36
Standard substance	SiO_2	Al_2O_3	Fe_2O_3	NaCl	KCl	$CaSiO_3$	ZnO	MgO
Percentage in ash [a] (%)	62.93	20.02	8.26	2.29	7.06	5.52	2.14	2.15

[a] Ash content was calculated from SSA (27.92%), and standard substance content was calculated from SSA surface.

From results of EDS analysis, apart from the basic elements (C, H, O, N and S), other elements was listed in Table 9. It confirmed that the SiO_2 was the main substance of SSA ash, with a percentage of 62.93%. It is noteworthy that the SSA contained a variety of metal elements (Al, Fe, K, Ca, Zn and Mg) on surface, which could form the active adsorption sites on SSA surface. Thus, the high inorganic mineral content of sewage sludge might be advantageous for SMP adsorption onto SSA. Eren *et al.* reported that the metal oxide influenced significantly the adsorption capacity of the bentonite in basic dye solution by ion exchange mechanism.[53,65] Compared to other adsorbates, the SSA possessed an excellent adsorption performance for the SMP, with a removal capacity of 39.41 mg g^{-1}. These results indicate that the SSA could be a new promising low cost adsorbent for removal of SMP in drilling wastewater.

4. Conclusion

In this study, a new adsorption performance of SSA was investigated for the removal SMP from aqueous solutions. The solution pH played a dramatic effect on the SMP adsorption onto SSA, and the maximum adsorption capacity of SMP onto SSA was obtained at pH of 2.4. Increasing electrolyte strength caused a small decrease in the adsorption capacity of SMP. The process of SMP adsorption onto SSA followed the pseudo-second-order kinetic model, and the intra-particle diffusion and film diffusion occurred simultaneously in the adsorption from intra-particle diffusion kinetic model. The adsorption was rightly described by Langmuir isotherm model, the monolayer adsorption capacity was estimated as 42.97 mg g^{-1}. Thermodynamic parameters were calculated, and the results indicated the adsorption was spontaneous and endothermic in nature. At 25 - 40 °C, the adsorption activation

energy (E_a) of 23.95 kJ mol^{-1} supported that the physisorption was more significant in the SMP-SSA system. Compared to other biochar and bentonitic adsorbents, SSA showed the highest adsorption capacity for SMP. These results indicated that the SSA could be a new promising low cost adsorbent for removal of SMP pollutants in drilling wastewater.

■ACKNOWLEDGMENTS

This study gained the financial support from National Natural Science Foundation of China (NO. 51104126), SWPU Pollution Control of Oil & Gas Fields Science & Technology Innovation Youth Team (No. 2013XJZT003), and Graduate Innovation Foundation of Southwest Petroleum University (No. CXJJ2015014).

■REFERNCES

1 A. Ros, M. A. Montes-Moran, E. Fuente, D. M. Nevskaia and M. J. Martin, *Environ. Sci. Technol*., 2006, 40, 302-309.

2 E. D. Revellame, R. Hernandez, W. French, W. E. Holmes, T. J. Benson, P. J. Pham, A. Forks and R. Callahan II, *RSC. Adv*., 2012, 2, 2015-2031.

3 T. Boualem, A. Debab, A. M. De Yuso and M.T. Izquierdo, *J. Environ. Manage*., 2014, 140, 145-151.

4 K.M. Smith, G. D. Fowler, S. Pullket and N. J. D. Graham, *Water Res*., 2009, 43, 2569-2594.

5 J. Bouzid, Z. Elouear, M. Ksibi, A. Feki and A. Montiel, *J. Hazard. Mater*., 2008, 152, 838-845.

6 M. Seredych and T. J. Bandosz, *J. Colloid Interface Sci*., 2006, 302, 379-388.

7 G. Gasco, A. Mendez and J. M. Gasco, *Desalination*., 2005, 180, 245-251.

8 Y. F. Jia and K. M. Thomas, *Langmuir*., 2000, 16, 1114-1122.

9 C. Gan, Y. Liu, X. Tan, S. Wang, G. Zeng, B. Zheng, T. Li, Z. Jiang and W. Liu, *RSC. Adv*., 2015, 5, 35107-35115.

10 M. Otero, F. Rozada, A. Moran, L. F. Calvo and A. I. Garcia, *Desalination*., 2009, 239, 46-57.

11 M. Otero, F. Rozada, L.F. Calvo, A. I. Garcia and A. Moran, *Biochem. Eng. J*., 2003, 15, 59-68.

12 Z. Wu, Y. Xiong, G. Guan, L. Kong and S. Tian, *RSC. Adv*., 2014, 4, 55256-55262.

13 C. Jindarom, V. Meeyoo, B. Kitiyanan, T. Rirksomboon and P. Rangsunvigit, *Chem. Eng. J*., 2007, 133, 239-246.

14 X. Fan and X. Zhang, *Mater. Lett*., 2008, 62, 1704-1706.

15 M. Seredych and T. J. Bandosz, *Ind. Eng. Chem. Res*., 2007, 46, 1786-1793.

16 L. Gu, N. Zhu, H. Guo, S. Huang, Z. Lou and H. Yuan, *J. Hazard. Mater*., 2013,

246-247, 145-153.
17 J. Rivera-Utrilla, C. V. Gomez-Pacheco, M. Sanchez-Polo, J. J. Lopez-Penalver and R. Ocampo-Perez, *J. Environ. Manage*., 2013, 131, 16-24.
18 R. Ding, P. Zhang, M. Seredych and T. J. Bandosz, Water Res., 2012, 46, 4081-4090.
19 G. Yang, H. Chen, H. Qin and Y. Feng, *App. Surf. Sci*., 2014, 293, 299-305.
20 V. M. Monsalvo, A. F. Mohedano and J. J. Rodriguez, *Chem. Eng. Res. Des*., 2012, 90, 1807-1814.
21 L. Kong, Y. Xiong, L. Sun, S. Tian, X. Xu and C. Zhao, *J. Hazard. Mater*., 2014, 274, 205-211.
22 L. Yu and Q. Zhong, *J. Hazard. Mater*., 2006, 137, 359-366.
23 Z. Pan, J. Tian, G. Xu, J. Li and G. Li, *Water Res*., 2011, 45, 819-827.
24 H. Zhang, R. Lv and S. Guo, *The Chinese Journal of Process Engineering*., 2007, 7, 718-722.
25 M. Li, Y. Guo, H. He, M. Lin, B. Peng and J. Guo, *Journal of China University of Petroleum*., 2010, 34, 145-149.
26 Z. Li, K. Liu, X. Cheng, K. Mei, F. Xiong and X. Guo, *J. Adhes. Sci. Technol*., 2015, 29, 1002-1013.
27 J. X. Guo, Y. J. Cui and J. J. Cao, *Pet. Sci*. 2013, 10, 106-111.
28 Y. Zhuang, Z. Zhu, H. Chao and B. Yang, *J. Appl. Polym. Sci*., 1995, 55, 1063-1067.
29 R. Lv and W. Jiang, *The Chinese Journal of Environmental Engineering*., 2002, 20, 3-5.
30 R. Lv, B. Mu, H. Zhang and S. Guo, *Pet. Sci*., 2008, 5, 275-279.
31 A.P.H.A, A.W.W.A, W.E.F., Standard Methods for the Examination of Water and Wastewater, 20th ed., American Public Health Association, Washington, DC, 1998.
32 ASTM D2867-09: Standard Test Methods for Moisture in Activated Carbon.
33 ASTM D2866-11: Standard test method for total ash content of activated carbon.
34 H. P. Boehm, *Carbon*., 2002, 40, 145–149.
35 L. Leng, X. Yuan, H. Huang, J. Shao, H. Wang, X. Chen and G. Zeng, *App. Surf. Sci*., 2015, 346, 223-231.
36 L. Sun, M. Li, M. Lin, B. Peng and J. Guo, *J. Disp. Sci. Tech*., 2009, 30, 605-608.
37 A. Ros, M. A. Lillo-Rodenas, C. Canals-Batle, E. Fuente, M. A. Montes-Moran, M. J. Martin and A. Linares-Solano, *Environ. Sci. Technol*., 2007, 41, 4375-4381.
38 Z. Pan, J. Tian, G. Xu, J. Lin and G. Li, *Water Res*., 2011, 45, 819-827.
39 Q. B. Wen, C. T. Li, Z. H. Cai, W. Zhang, H. L. Gao, L. J. Chen, G. M. Zeng, X. Shu and Y. P. Zhao, *Biores. Technol*., 2011, 102, 942-947.

40 O. Duggan and S. J. Allen, *Wat. Sci. Tech*., 1997, 35, 21-27.

41 M.-J. Jung, K.-H. Ahn, Y. Lee, K.-P. Kim, J.-S. Rhee, J.-T. park and K.-J. Paeng, *Microchem. J*., 2001, 70, 123-131.

42 J. Zhang and P. Zheng, *RSC. Adv*., 2015, 5, 17768-17774.

43 S. B. Choi and Y. S. Yun, *J. Hazard. Mater*., 2006, 138, 378-383.

44 W. Shen, Z. Li and Y. Liu, *Recent Pat. Chem. Eng*., 2008, 1, 27-40.

45 M. S. Akhter, J. R. Keifer, A. R. Chughtai and D. M. Smith, *Carbon*., 1985, 23, 589-591.

46 B. J. Meldrum and C. H. Rochester, *J. Chem. Soc., Faraday Trans*., 1990, 86, 861-865.

47 E. Raymundo-Pinero, D. Cazorla-Amoros and C. S. M. De Lecea, *Carbon*., 2000, 38, 335-344.

48 J. Przepiorski, *J. Hazard. Mater*., 2006, 135, 453-456.

49 L. Yu and Q. Zhong, *J. Hazard. Mater*., 2006, 137, 359-366.

50 B. K. Nandi, A. Goswami and M. K. Purkait, *J. Hazard. Mater*., 2009, 161, 387-395.

51 X. Liu and N. Pinto, *Carbon*., 1997, 35, 1387-1397.

52 E. Eren and H. Gumus, *Desalination*., 2011, 273, 276-284.

53 E. Eren, *J. Hazard. Mater*., 2009, 162, 1355-1363.

54 M. Alkan, O. Demirbas, S. Celickcapa and M. Dogan, *J. Hazard. Mater*., 2004, B116, 135-145.

55 C. Dwivedi, S. K. Pathak, M. Kumar, S. C. Tripathi and P. N. Bajaj, *RSC. Adv*., 2013, 3, 22102-22110.

56 Y. S. Ho and G. Mckay, *Proc. Biochem*., 1991, 34, 451-465.

57 K. Lin, J. Pan, Y. Chen, R. Cheng and X. Xu, *J. Hazard. Mater*., 2009, 161, 231-240.

58 C. H. Wu, *J. Hazard. Mater*., 2007, 144, 93-100.

59 H. Nollet, M. Roels, P. Lutgen, P. Van der Meeren and W. Verstraete, *Chemosphere*., 2003, 53, 655-665.

60 M. Kara, H. Yuzer, E. Sabah and M. Celik, *Water Res*., 2003, 37, 224-232.

61 I. Vazquez, J. Rodriguez-Iglesias, E. Maranon, L. Castrillon and M. Alvarez, *J. Hazard. Mater*., 2007, 147, 395-400.

62 J. Yan, *Journal of Southwest Petroleum University Institute*., 1982, 1, 26-36.

63 E. Eren, O. Cubuk, H. Ciftci, B. Eren and B. Caglar, *Desalination*., 2010, 252, 88-96.

64 T. Grant and C. King, *Ind. Eng. Chem. Res*., 1990, 29, 264-271.

65 E. Eren and B. Afsin, *Dyes Pigments*., 2007, 73, 162-167.